Journal of Power Sources 192 (2009) 674–678

Contents lists available at ScienceDirect

Journal of Power Sources

journal homepage: www.elsevier.com/locate/jpowsour

Short communication

Relationship between carbon corrosion and positive electrode potential in a proton-exchange membrane fuel cell during start/stop operation

Jutae Kim, Junhee Lee, Yongsug Tak*

Department of Chemical Engineering, Inha University, Incheon 402-751, Republic of Korea

ARTICLE INFO

Article history:
Received 30 December 2008
Received in revised form 2 March 2009
Accepted 8 March 2009
Available online 27 March 2009

Keywords:
Polymer electrolyte membrane fuel cell
Carbon support corrosion
Fuel starvation
Start-up/shut-down

ABSTRACT

Fuel starvation during start-up and shut-down processes can adversely affect the performance of proton-exchange membrane fuel cells. In this study, fuel starvation is induced intentionally by supplying hydrogen and air to the negative electrode (anode) side alternately, and the individual electrode potential is measured *in situ* using a dynamic hydrogen electrode. The positive electrode (cathode) potential is increased to 1.4 V when air/hydrogen boundaries developed on the anode side. The development of a high cathode potential causes oxidation of the carbon support with the amount of CO_2 evolution proportional to the cathode potential above 1.0 V. Above ~1.2 V, CO and SO_2 are generated electrochemically or chemically and the rate of CO production is higher than that of SO_2. Although a higher cathode potential is induced irrespective of the cell temperature, oxidation of the carbon support is retarded significantly at low temperatures.

1. Introduction

Proton-exchange membrane fuel cells (PEMFCs) have been investigated as sustainable energy sources for electrical vehicles and residential power generation. However, PEMFCs are confronted with a lack of reliability and durability under low-temperature operation and fuel starvation during the start-up and shut-down processes. These adverse conditions deteriorate the electrode materials during long-term operation and thereby limit the commercialization of PEMFCs.

PEMFCs employ carbon as a catalyst support for the Pt electrode because it has a high surface area and good chemical stability. Since carbon has a low equilibrium potential for carbon corrosion, as shown in the following reactions:

$$C + 2H_2O \rightarrow CO_2 + 4H^+ + 4e^-, E^0 = 0.207\,\text{Vvs.SHE} \quad (1.1)$$

$$C + H_2O \rightarrow CO + 2H^+ + 2e^-, E^0 = 0.518\,\text{Vvs.SHE} \quad (1.2)$$

it can be thermodynamically unstable at potentials above equilibrium potential. Although the rate of carbon oxidation is negligible during normal operation of PEMFCs [1], it has been suggested that carbon corrosion can occur at potentials greater than the open-circuit voltage (OCV) [2,3]. The OCV of a cell is close to the potential of the positive electrode (cathode) because the overpotential for the negative electrode (anode) reaction is quite low. Previous studies examined carbon corrosion in a half-cell test and reported that carbon oxidation occurs above 1.0 V vs. SHE [4–7]. The cathode potential increases to a high potential when fuel starvation occurs on the anode side during the start-up and shut-down processes, resulting in corrosion of the cathode carbon support [8–11]. The potential shift to a higher value on the cathode was attributed to the existence of air/fuel boundary on the anode [2]. Direct *in situ* measurements of the cathode potential during fuel starvation of a PEMFC was recently reported [12] but the relationship between the cathode potential and carbon oxidation was not fully examined.

In this study, a dynamic hydrogen electrode (DHE) is installed as a reference electrode inside a PEMFC and used to measure the individual anode and cathode potentials *in situ* during diverse operations of the cell. The effect of fuel starvation on the cell performance and carbon oxidation is examined by intentionally constructing an air/fuel boundary by blowing air into the anode gas channel. The cathode potential is measured continuously during fuel starvation and the gas products produced on the cathode side are identified and analyzed quantitatively using a FT-IR spectrometer connected to the fuel cell system. The direct relationship between the cathode potential and the formation of gaseous products, i.e., CO_2, CO and SO_2, is investigated.

2. Experimental

The performance tests were carried out using a single cell with a membrane electrode assembly (MEA) with an active area of 25 cm^2. The MEA had a platinum loading of 0.4 mg cm^{-2} on both the anode and cathode sides and a membrane thickness of 18 μm.

* Corresponding author. Tel.: +82 32 866 0587; fax: +82 32 866 0587.
E-mail address: ystak@inha.ac.kr (Y. Tak).

0378-7753/$ – see front matter © 2009 Elsevier B.V. All rights reserved.
doi:10.1016/j.jpowsour.2009.03.039

An edge-type dynamic hydrogen electrode (DHE) was installed on membrane to investigate the individual electrode potential behaviour during fuel starvation [13–15]. Two electrodes of DHE were made of 0.2 mm Pt wires and placed on the cathode side near the air/hydrogen inlet. Before the measurements, hydrogen was supplied to the anode and the potential between the DHE and anode was adjusted to zero by controlling the current of the DHE system.

Fig. 1 shows the profile of the hydrogen gas flow rate for an accelerated fuel starvation operation experiment of the PEMFC. Sufficient hydrogen (99.999% hydrogen) fuel was supplied to the anode and a stable OCV of ~0.9 V was obtained at t_1. The hydrogen supply was stopped at t_1 and 30 ml min^{-1} of air (20.9% O_2 in N_2) at STP (standard temperature and pressure) was forced into anode side. When the cell potential decreased to 0.1 V at t_2, the air supply was interrupted and the hydrogen gas supply was resumed. The air (20.9% O_2 in N_2) flow rate to the cathode was maintained at 30 ml min^{-1} during the fuel-starvation experiment. The effects of the fuel-starvation temperature on the carbon oxidation and cell performance were investigated.

The potentials of the anode and cathode were measured *in situ* with a DHE, and the cell potential was recorded simultaneously using a multi-channel voltage logger (Graphtec, GL500). The product gases generated on the cathode during fuel starvation were identified and analyzed using a Fourier Transform Infrared Spectrometer (FT-IR, Photal IG-2000) installed at the cathode outlet. The cell performance was interpreted from the current–voltage curves using electronic loads (Daegil Electronics, EL 500P). The impedance spectra were measured at the OCV using a potentiostat and galvanostat/log-in amplifier (Zahner, IM6). The frequencies investigated ranged from 2 kHz to 40 mHz with a ±5 mV amplitude. During the current–voltage test and impedance operation, the cell temperature was set to 70 °C and the inlet gases were fully humidified. The thickness of the cathode layer was measured from field emission scanning electron microscopy images (FE-SEM, Hitach S-4300).

3. Results and discussion

Fig. 2 shows the cell voltage and electrode potential relative to the DHE during the transition from normal operation to accelerated fuel starvation. Simultaneously, the potential of the DHE was recorded to identify the stable operation irrespective of the harsh environments around the DHE, such as fuel starvation. Fuel starvation limits the production of protons and, consequently, the

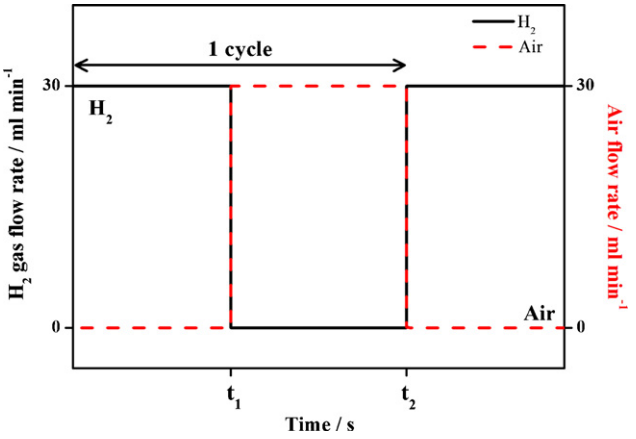

Fig. 1. Profile of hydrogen gas flow rate during accelerated fuel starvation experiment. At t_1, 30 ml min^{-1} of air is forced into the anode side and hydrogen gas flow rate is resumed at t_2.

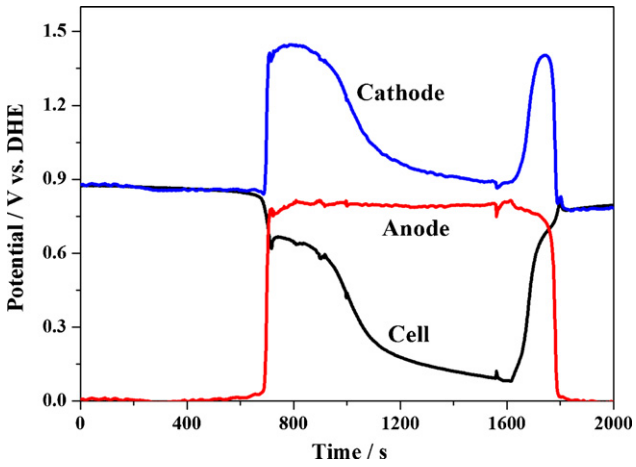

Fig. 2. Direct measurements of cell potential and electrode potential with DHE.

electro-osmotic drag of water and protons to the cathode reduces the concentration of protons on the anode side of the membrane. When the DHE is placed on the anode side, the insufficient amount of protons limits the mass transfer of protons to the DHE and the applied current to the DHE system dissociates the water inside the membrane to hydrogen. The dissociation of water can cause a sudden change in the potential of the DHE system, so that it may not be able to provide a reference point for measuring the electrode potential. When the DHE is located on the cathode side, its potential is maintained at a constant value, irrespective of the substantial change in cell voltage due to fuel starvation. The steady potential of the DHE provides a stable reference point for measurements of the individual electrode potential.

When air flows into an anode channel filled with hydrogen fuel, the cathode potential increases rapidly to 1.4 V and then decreases slowly; potential remains above 1.0 V for more than 500 s, as shown in Fig. 2. The cell potential remains at the OCV for 700 s after supplying air to anode because air must pass through the humidifier and connecting tubes. The increase in the potential of the anode and cathode at 700 s indicates that oxygen/hydrogen boundaries begin to form at the anode channel of the cell. Simultaneously, a decrease in cell potential is observed because of the decreased hydrogen concentration inside the cell. When the cell potential reaches 0.1 V at 1550 s, hydrogen fuel is re-supplied to the anode filled with air. The oxygen/hydrogen boundaries are reformed on the anode channel and a high cathode potential is induced. On the other hand, the increase in hydrogen fuel results in a high cell voltage, but only for a short period because the fast transport of hydrogen rapidly removes the air/fuel boundary area, relative to air introduction to an anode filled with hydrogen.

The higher induced cathode potential can be interpreted as oxidation of the cathode carbon support. The FT-IR spectrum in Fig. 3 indicates that CO_2 generation occurs during fuel starvation. By contrast, CO_2 is not detected during normal fuel-rich operation.

The anode potential also shifts to a higher value as a result of the cathodic reaction due to the presence of oxygen on the anode, i.e., $O_2 + 4H^+ + 4e^- \rightarrow 2H_2O$. Nevertheless, the cell voltage decreases slowly, as shown in Fig. 2. Previous mathematical modelling has suggested that the cathode potential increases with increasing air/fuel boundary area on the anode [2,3]. The data in Fig. 2 also shows that the air/fuel boundary exists for more than 10 min.

The relationship between the gas concentration in the cathode outlet and the cathode potential is presented in Fig. 4. The concentration profile of CO_2 resembles the cathode potential transients. The gas concentrations are analyzed from the following FT-IR

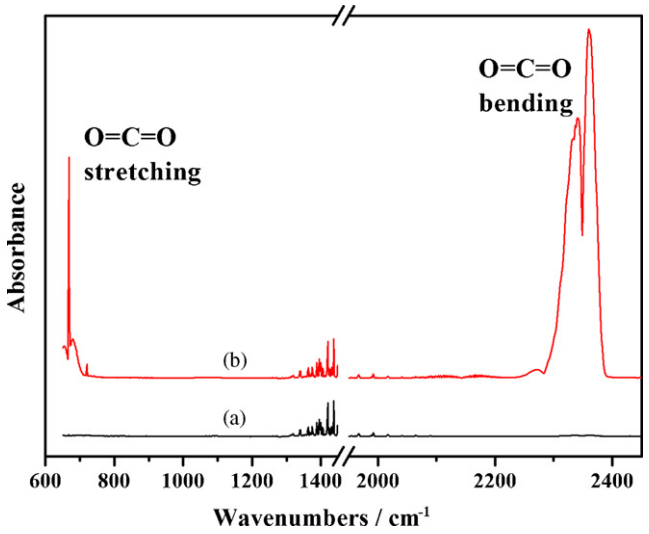

Fig. 3. FT-IR spectra of gases out the cathode outlet: (a) normal operation and (b) fuel starvation.

absorbance peaks: CO_2 at 2280–2390 cm^{-1} and 613–725 cm^{-1}, CO at 1985–2260 cm^{-1}, and SO_2 at 1290–1415 cm^{-1}. Low CO_2 concentrations <1000 ppm are analyzed from the absorbance peak area at 2280–2390 cm^{-1} and high CO_2 concentrations >1000 ppm are obtained from the 613–725 cm^{-1} peak because the absorbance peak area shows a linear relationship with the CO_2 concentration in these wave number ranges, as shown in Fig. 5. The FT-IR spectra were collected every 8 s and converted to ppm. The distance

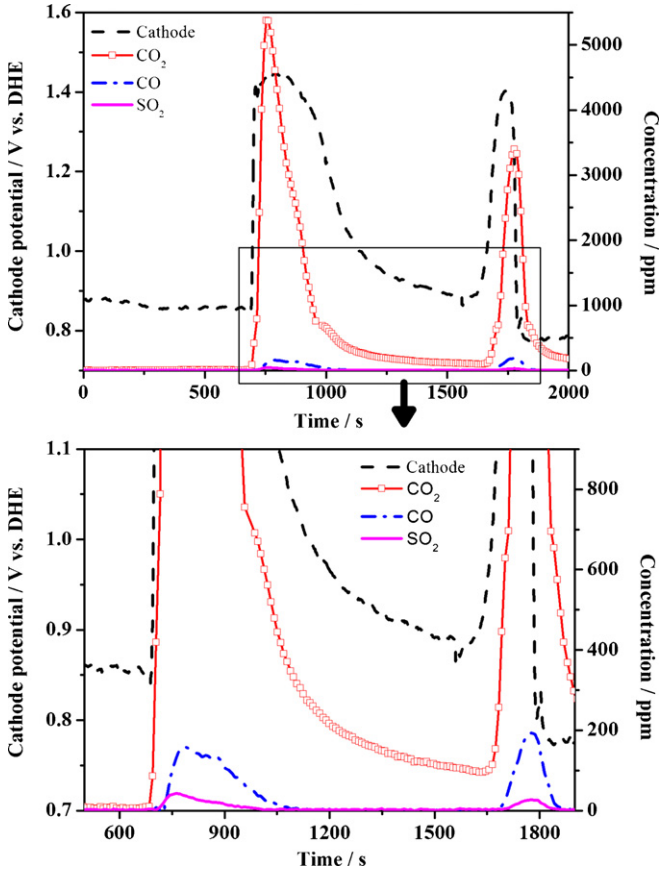

Fig. 4. Quantitative analysis of cathode outlet gases with change in cathode potential.

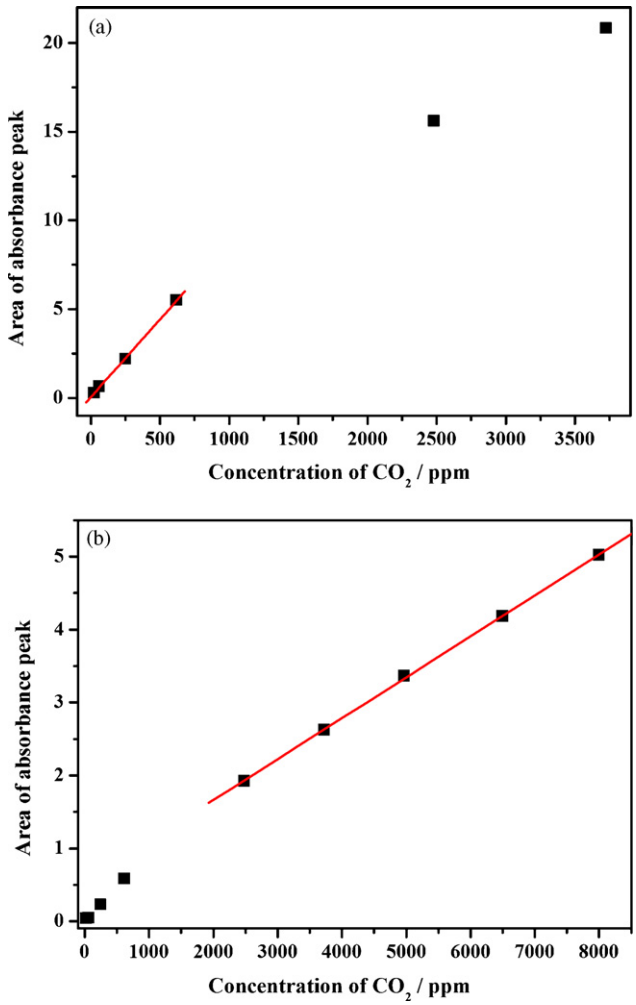

Fig. 5. Relationship between concentration of CO_2 and absorbance peak area at different wave number ranges. (a) 2280–2390 cm^{-1} and (b) 613–725 cm^{-1}, respectively.

between the cathode outlet and FT-IR detector allows the axial dispersion of gas along the gas tube, which can cause a long tail of CO_2.

With respect to electrochemical kinetics, it can be assumed that the highest concentration of CO_2 by reaction (1.1) is produced at the highest potential. By coinciding this highest concentration and potential on the graph, the concentration of CO_2 is definitely a function of the cathode potential above ~1.0 V, and the CO_2 tail below 1.0 V may be due to dispersion along the flow path to the detector. The production of CO by reaction (1.2) begins after that of CO_2. The amount of CO production is quite low, as shown in Fig. 4. The delayed formation of CO can be interpreted by the requirement of a higher potential above ~1.2 V. The production of CO is quite important because it poisons the active sites of the cathode Pt catalyst. Surprisingly, SO_2 is detected at the potential range of CO generation but its amount is far less than CO. The source of SO_2 may be either sulfur on the carbon surface or the sulfonate group ($-SO_3^-$) of the Nafion membrane and ionomer. This indicates that a potential >1.2 V can induce local heating of the membrane, and the resulting increase in temperature can generate SO_2 through decomposition of the membrane [16,17]. Nevertheless, the exact source of sulfur dioxide is unclear. An analysis of the gas products during fuel starvation indicates that the main product of carbon oxidation is CO_2, with CO as a by-product. The loss of the carbon support may cause the mechanical removal of Pt nanoparticles and significantly decrease the efficiency of the Pt electrocatalyst.

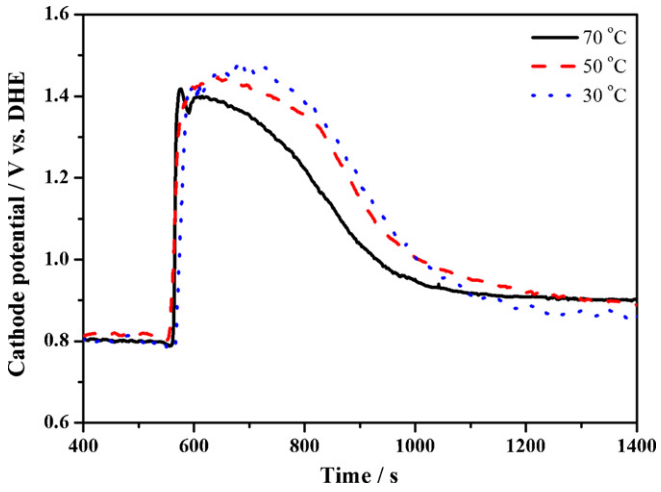

Fig. 6. Effect of cell temperature on increase in cathode potential during air inlet to anode channel.

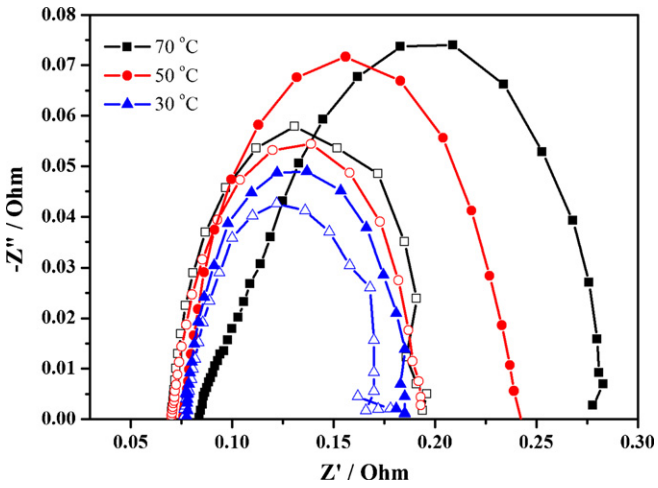

Fig. 8. Nyquist plots for measured impedance of fuel cell. Open symbols were obtained before applying fuel starvation cycle and close symbols represent the effects of 9 cycles of fuel starvation at different temperatures.

The effect of the fuel starvation temperature on the increase in cathode potential is shown in Fig. 6. The potential transients are little affected by the fuel starvation temperature. On the other hand, the data in Figs. 7 and 8 suggest that after successive 9 cycles of fuel starvation in Fig. 1 at different temperatures, the deterioration of the cell performance is quite severe at 70 °C but relatively mild at 30 °C. Electrochemical impedance spectra were measured to understand the difference between zero and nine cycles of fuel starvation at different temperatures. The high-frequency resistance corresponds to the ohmic resistance and can be attributed primarily to the membrane resistance in a fuel cell system. The low-frequency resistance represents the charge-transfer resistance at electrode catalysis. Fig. 8 shows the comparative impedance spectra (open symbols) measured before fuel starvation test and after the 9 cycles (closed symbols) at different temperatures. After 9 cycles of fuel starvation, the charge transfer resistance increases by 56.7% at 70 °C but it only increases by 19.9% at 30 °C. The slow rate of CO_2 electrochemical oxidation at low temperatures may be responsible for the reduced deterioration of the cell performance, even at a higher cathode potential.

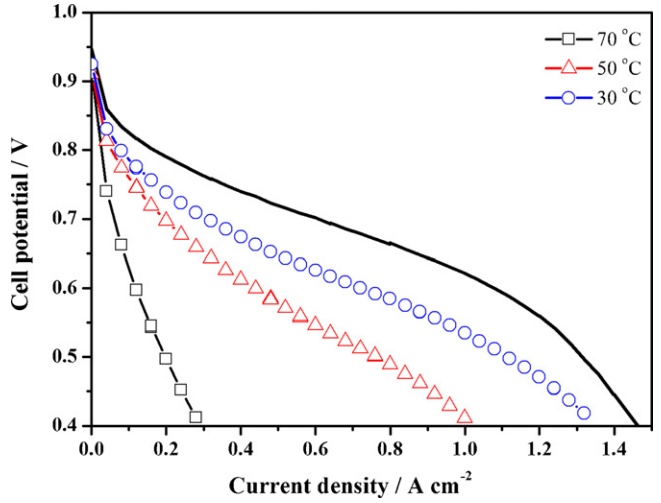

Fig. 7. Effect of fuel starvation temperature on current–potential curves. Cell performance tested at 70 °C. Line plot is obtained before applying fuel starvation cycle. Open symbols represent the effects of the 9 cycles of fuel starvation at different temperatures.

The change in OCV at zero current after fuel starvation is shown in Fig. 7. The impedance measurements at high frequency in Fig. 8 indicate that the membrane resistance increases as a result of fuel starvation both at 50 °C and at 70 °C. An increase in membrane resistance due to the blocking of the proton pathways of the membrane can be related to deterioration of the membrane by the evolution of SO_2 during the acceleration test.

The peak CO_2 concentration of each fuel starvation cycle when air is instilled into the H_2-filled channel is shown in Fig. 9. At 30 °C, the CO_2 concentration is almost constant regardless of the fuel starvation cycle number. The rate of CO_2 generation is high, however, and increases rapidly during the initial two cycles at 70 °C. This means that the first cycle activates carbon corrosion on the active catalyst site. Further cycles of fuel starvation reduce the absolute amount of carbon through conversion to CO_2 and CO, and the concomitant removal of Platinum may decrease the level of CO_2 evolution.

Fig. 10 shows that the thickness of the cathode layer measured near the middle parts of MEAs decreases with increasing number of fuel starvation cycles at 70 °C. The thickness reduction is greatest during the initial fuel starvation cycle, which coincides with the CO_2 evolution rate shown in Fig. 9. Even after OCV operation for 15 h, however, there is no decrease in OCV, no increase

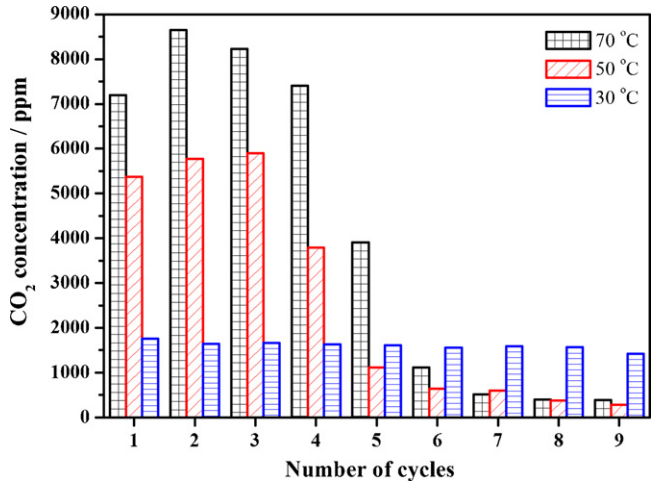

Fig. 9. CO_2 generation from cathode carbon support with successive cycles of fuel starvation.

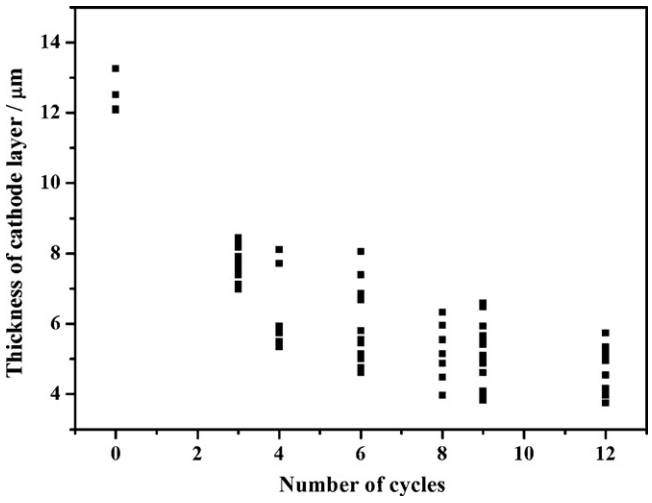

Fig. 10. Thickness variation of cathode layer after successive cycling of accelerated fuel starvation.

in membrane resistance, and no thickness variation of the catalyst layer.

4. Conclusions

The effect of fuel starvation on cell performance and carbon oxidation is determined by intentionally inducing fuel starvation by blowing air into the anode gas channel. A dynamic hydrogen electrode is installed as a reference electrode on the cathode side of the PEMFC and used for the *in situ* measurements of the individual anode and cathode potential during fuel starvation. Direct measurements of the cathode potential and gas analysis by FT-IR clearly suggest that an induced high cathode potential causes oxidation of the carbon support, and thereby degrades the fuel cell performance. The amount of CO_2 evolved is proportional to the cathode potential above 1.0 V. CO and SO_2 are generated either electrochemically or chemically above ~1.2 V, and are detrimental to cell performance. Although a higher cathode potential was induced irrespective of the cell temperature, oxidation of the carbon support is retarded significantly at low temperatures.

Acknowledgment

This work was supported by New & Renewable Energy R&D program (2004-N-FC12-P-01-0-000) under the Korea Ministry of Commerce, Industry and Energy (MOCIE).

References

[1] B.J. Eastwood, P.A. Christensen, R.D. Armstrong, N.R. Bates, J. Solid State Electrochem. 3 (1999) 179.
[2] J.P. Meyers, R.M. Darling, J. Electrochem. Soc. 153 (2006) A1432.
[3] C.A. Reiser, L. Bregoli, T.W. Patterson, J.S. Yi, J.D. Yang, M.L. Perry, T.D. Jarvi, Electrochem. Solid State Lett. 8 (2005) A273.
[4] A.M. Chaparro, N. Mueller, C. Atienza, L. Daza, J. Electroanal. Chem. 591 (2006) 69.
[5] J. Wang, G. Yin, Y. Shao, S. Zhang, Z. Wang, Y. Gao, J. Power Sources 171 (2007) 331.
[6] K.H. Kangasniemi, D.A. Condit, T.D. Jarvi, J. Electrochem. Soc. 151 (2004) E125.
[7] L.M. Roen, C.H. Paik, T.D. Jarvi, Electrochem. Solid State Lett. 7 (2004) A19.
[8] H. Tang, Z. Qi, M. Ramani, J.F. Elter, J. Power Sources 158 (2006) 1306.
[9] T.F. Fuller, G. Gray, ECS Transactions 1 (2006) 345.
[10] H. Chizawa, Y. Ogami, H. Naka, A. Matsunaga, N. Aoki, T. Aoki, ECS Transactions 3 (2006) 645.
[11] P.T. Yu, W. Gu, R. Makharia, F.T. Wagner, H.A. Gasteiger, ECS Transactions 3 (2006) 797.
[12] W.R. Baumgartner, P. Parz, S.D. Fraser, E. Wallnöfer, V. Hacker, J. Power Sources 182 (2008) 413.
[13] A. Küver, I. Vogel, W. Vielstich, J. Power Sources 52 (1994) 77.
[14] G. Li, P.G. Pickup, Electrochim. Acta 49 (2004) 4119.
[15] Z. Siroma, R. Kakitsubo, N. Fujiwara, T. Ioroi, S.I. Yamazaki, K. Yasuda, J. Power Sources 156 (2006) 284.
[16] S.R. Samms, S. Wasmus, R.F. Savinell, J. Electrochem. Soc. 143 (1996) 1498.
[17] C.A. Wilkie, J.R. Thomsen, M.L. Mittleman, J. Appl. Polym. Sci. 42 (1991) 901.